Optical torque induces magnetism at the molecular level

M. **T**uan **T**rinh[1*], **K**rishnandu **M**akhal[1], **E**lizabeth **F.C. D**reyer[1], **A**poorv **S**hanker[2], **S**eong-**J**un **Y**oon[2], **J**insang **K**im[2], and **S**tephen **C. R**and[1,3]

[1]*Dept. of Electrical Engineering, University of Michigan, Ann Arbor, MI 48109*
[2]*Dept. of Materials Science, University of Michigan, Ann Arbor, MI 48109*
[3]*Dept. of Physics, University of Michigan, Ann Arbor, MI 48109*
**tuantrin@umich.edu*

Abstract: We report experimental observations of a mechanism that potentially supports and intensifies induced magnetization at optical frequencies without the intervention of spin-orbit or spin-spin interactions. Energy-resolved spectra of scattered light, recorded at moderate intensities (10^8 W/cm^2) and short timescales (<150 fs) in a series of non-magnetic molecular liquids, reveal the signature of torque dynamics driven jointly by the electric and magnetic field components of light at the molecular level. While past experiments have recorded radiant magnetization from magneto-electric interactions of this type, no evidence has been provided to date of the inelastic librational features expected in cross-polarized light scattering spectra due to the Lorentz force acting in combination with optical magnetic torque. Here, torque is shown to account for unpolarized rotational components in the magnetic scattering spectrum under conditions that produce only polarized vibrational features in electric dipole scattering, in excellent agreement with quantum theoretical predictions.

1. Introduction

For several decades, interactions that couple electric and magnetic effects in bulk materials through magnetostriction and piezoelectricity have been the subject of intense investigation. Such interactions operate either by magnetostriction in a material which generates an internal piezo-electric field in response to the deformation or by the reverse process. They are of great potential value for energy conversion and novel sensor technology. Consequently, there is considerable interest in creating multifunctional circuits based on magneto-electric and multiferroic materials that combine electronic and magnetic properties [1-9]. To date, however, such devices have relied on the properties of bulk magnetic solids or magnetic thin films, making them difficult to miniaturize. The control of magnetism in nanoscale or molecular level is of great interest for the advancement of nanotechnology. Yet, there have been no reports of induced magnetism in non-magnetic materials on the nanoscale. While magneto-electric interactions on nanoscale or molecular level have been discussed in the literature [10-12], and recently observed [13] and theorized [14,15], no detailed confirmation of the theoretical torque mechanism proposed to explain how these effects undergo strong enhancement has been published. At non-relativistic intensities of light, possible effects of the optical magnetic field are normally dismissed owing to the smallness of the Lorentz driving force qvB (proportional to the velocity v of a charge q) compared to the electric force qE. Since $B<<E$, this would be perfectly justified if no enhancement mechanism existed to magnify the Lorentz force of light. However, a fundamental mechanism exists that is capable of enhancing magnetism induced jointly by the optical fields E and H at the level of individual molecules [14, 15]. In magneto-

electric interactions, orbital angular momentum can be converted to molecular rotational angular momentum, enlarging the effective area enclosed by displacive currents. As a result, the magnetic dipole moment becomes enhanced. In this paper, we present the first direct experimental evidence that torque by the optical magnetic field, thought to be capable of enhancing radiant magnetization to the same level as electric dipole polarization at optical frequencies under non-relativistic conditions[13-15], does indeed accompany magneto-electric interactions at the molecular level.

Here, ultrafast magnetic response was studied in pulsed optical experiments using a simple 90^o scattering geometry (Fig. 1(a)). Despite the extensive literature on depolarized light scattering [16-22], there have been few reports of the complete radiation patterns or inelastic spectra that are necessary to distinguish between electric dipole (ED) and magnetic dipole (MD) response at the molecular level. Early studies of collisional effects in gases and liquids showed that they generated a small amount of depolarization even in isotropic molecules at low light intensities, on relatively long timescales (i.e. timescales exceeding the collisional reorientation time). However, no experiments were performed at high enough intensities or sufficiently short timescales to discriminate between collisional depolarization and magnetization on the basis of the angular distribution of scattered radiation or by performing suitable spectral analysis. In the present work, we utilized moderately high intensities (up to $I \sim 10^8 W/cm^2$) and ultrashort pulses ($\tau_p < 150$ *fs*) to record both the radiation patterns and spectrally-resolved inelastic features in polarization-analyzed scattered light. Our experimental results disclose key details of the mechanism governing radiant optical magnetization in dielectric media for the first time.

The magnitude of an induced magnetic dipole moment m is normally limited to a small fraction of the induced electric dipole p, namely $(m/p) < \alpha$, where $\alpha = 1/137$ is the fine structure constant. Exceptions occur in media where spin-spin interactions are strong or the ED approximation is not upheld, such as in ferromagnets, structured dielectrics, metamaterials, and nanoparticles. However, strong induced magnetic response has not been anticipated in natural homogeneous (non-magnetic) materials at high frequencies. For this very reason, highly engineered, non-uniform metamaterials have attracted much attention as an important way to realize magnetic response through structural design. In the present work, however, the mechanism of an intriguing alternative is explored. Dynamic magneto-electric interactions are tested as a route for superseding traditional limitations on induced magnetic moments, and are found to agree with classical simulations [14] and quantum theory [15] predicting that magnetic optical torque can create and enhance magnetic response in nominally non-magnetic media through an ultrafast exchange of orbital and rotational angular momenta.

2. Methods and Results

Our experimental setup utilized an amplified femtosecond laser system (Amplitude Inc.) operating at 800 nm and delivering pulses of up to 0.5 mJ at a rate of 10 kHz over an electronically-tunable bandwidth of 15 to 100 nm. Intensities in the range of 10^7-10^8 W/cm^2 per pulse were typically used in a collimated beam 5 mm in diameter to induce and probe magnetic response of dielectric materials. Samples consisted of a series of tetrahedral molecular liquids, including CCl_4, $SiCl_4$, $SiBr_4$, $Si(OCH_3)_4$, and $Si(OC_2H_5)_4$. These molecules exhibit isotropic optical response at low powers and represent a series in which the moment of inertia increases systematically. Complete radiation patterns were recorded in co-polarized and cross-polarized light-scattering geometries at 90^o with respect to the incident beam by rotating the input polarization angle θ through 360 degrees under computer control [13]. A schematic of the setup and a typical set of raw data for co- and cross-polarized signals for CCl_4 are shown in Figs. 1(a) and 1(b). The corresponding radiation patterns are plotted in Fig. 1(c), after subtraction of the unpolarized components (constant backgrounds) shown in Fig. 1(b). The dependence on the input intensity of the scattering light was previously shown to be quadratic at low intensities

[13]. Radiation patterns for all samples showed the same depolarized and dipolar components with low residuals as in CCl_4.

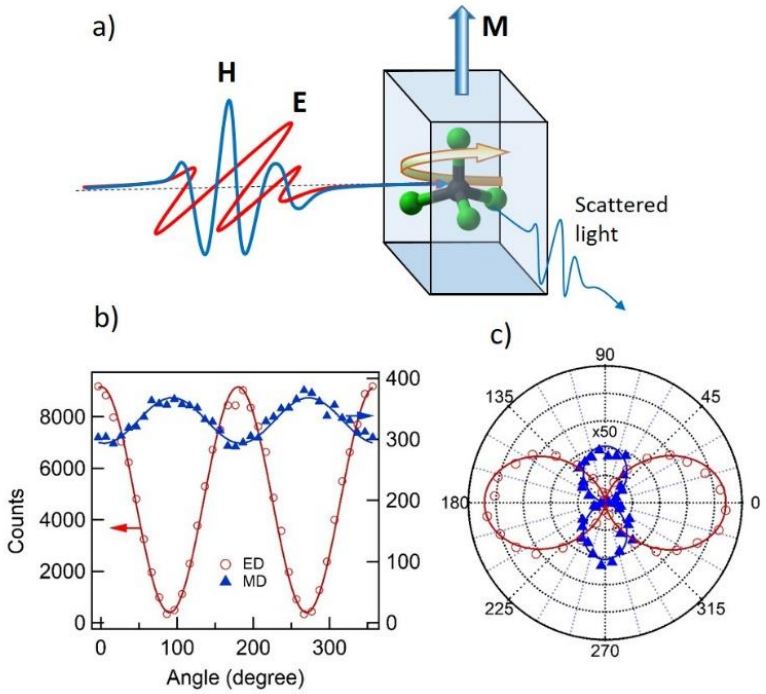

Fig. 1. (a) The light scattering process: the optical electric field causes an electric dipole transition which imparts orbital kinetic energy to the molecule. This energy is subsequently converted to librational motion by the optical magnetic field. The induced electric and magnetic dipole moments cause incoherent scattering at an angle to the incident beam. (b) Raw data for co-polarized (circles) and cross-polarized (triangles) scattering intensities versus input rotation angle in CCl_4. (c) Radiation patterns of the co- and cross-polarized light-scattering data after subtraction of the constant (unpolarized) background evident in Fig. 1(b). The solid curves are fits to a $\cos^2\theta$ function.

A key result of this work is shown in Fig. 2, which displays the normalized co-polarized and cross-polarized spectra of scattered light in CCl_4 recorded with a 0.5 m grating spectrometer. These spectra are labelled ED and MD, respectively. The co-polarized (Rayleigh scattering) spectrum in red is virtually indistinguishable from the instrumental response over the bandwidth reflecting the pulse duration (see the inset of Fig. 2). The cross-polarized spectrum in blue has large additional features in it. These features may be emphasized by subtracting the co-polarized signal to obtain the difference spectrum shown in grey. The extra features appearing in the cross-polarized spectrum are then found to correspond to inelastic scattering from known rotations and vibrations of individual CCl_4 molecules. Below the grey curve are the expected positions and relative weights of rotationally- and vibrationally-shifted satellite lines, indicated by vertical bars displaced from the origin (downward arrow at the peak of the pulse spectrum). Co- and cross-polarized spectra for the other samples are shown in Figs. 3(a)-6(c). Experimental values of the rotation and vibration energies were determined from a best fit convolution of the instrumental response $I(\omega)$ with an assumed spectrum of satellite lines of variable height and position. The width of these features was assumed to be instrument-limited. The results for fitted vibration and rotation frequencies in Fig. 2 are in good agreement with literature values [24,25]. The comparison of experimental rotation frequencies with results from prior spectroscopy shown in Fig. 3(d) provides compelling evidence for our rotational assignments and confirms that rotations (or more correctly librations) are generated exclusively

during the interaction responsible for cross-polarized scattering. That is, unpolarized rotational features are notably absent from the ED spectrum.

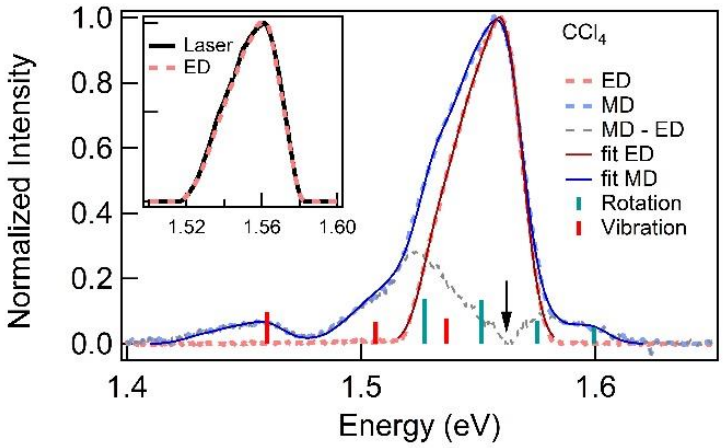

Fig. 2. Normalized co- and cross-polarized scattered light spectra in CCl_4, dashed-red (labelled ED) and -blue (labelled MD), respectively. The black arrow indicates the spectral peak. The solid curve showing a best fit that takes instrumental linewidth into account together with inelastic components due to vibrational and rotational transitions as indicated by vertical red and blue bars. The grey curve is the difference between the red and blue curves, highlighting the inelastic components in the MD spectrum. Inset: A comparison of the laser and ED spectra.

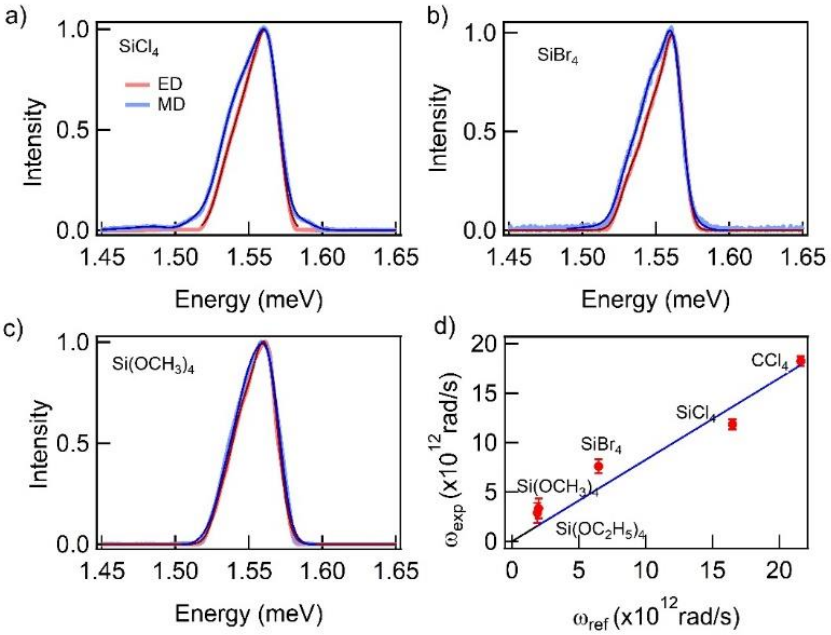

Fig. 3. Normalized co- and cross-polarized scattered light spectra for various compounds. (a) $SiCl_4$, (b) $SiBr_4$ and c) $Si(OCH_3)_4$ with fitted curves. (d) The experimental rotation frequencies (ω_{exp}) plotted versus literature values (ω_{ref}) [24, 25] for all samples. The solid line is a linear fit with a slope of 0.85.

Further measurements supported the 2-photon picture of the interaction hypothesized in [14, 15]. The results of analyzing polarization states of the inelastic scattered light components are shown in Fig. 4 and agree with expectations based on the two downward transitions

displayed in Fig. 5(a). Complete scattered light spectra were recorded at values of θ separated by discrete steps of 30° to determine whether particular spectral features were polarized, unpolarized or of mixed polarization. In Fig. 4(a), the elastic component at the center of the cross-polarized (MD) spectrum dropped by 30% as the input field was rotated away from horizontal (90°). This result indicated that it was partially polarized, composed of both a dipolar contribution to scattered light and a large unpolarized background (also consistent with Fig. (1b)). Spectral features at large shifts (1.4 to 1.53 eV) on the other hand did not vary at all as the input polarization was varied. This is shown on the left side of Fig. 4(a) where the curves for different input polarizations are all overlapped. These features were completely unpolarized. In the next section, we discuss in more detail the close correspondence of these findings with expectations from the quantum theory of magneto-electric interactions at the molecular level.

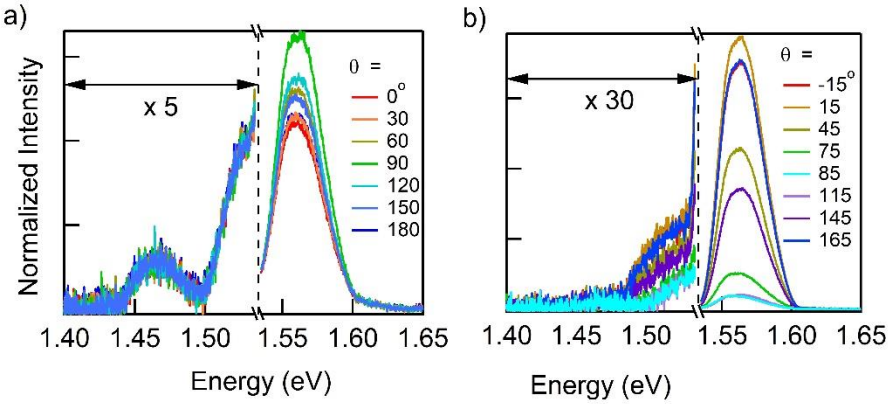

Fig. 4. Polarization dependence of cross-polarized (a) and co-polarized (b) spectra in CCl_4. θ is the pump polarization angle. The input angle $\theta = 0°$ corresponds to vertical polarization. In (b) the entire spectrum is highly polarized, including small vibrational features due to spontaneous Raman scattering (see variation of curves with input polarization at low energies). The energy range from 1.40 to 1.53 eV has been magnified 5 times for (a) and 30 times for (b).

3. Discussion

Many physical processes cause depolarization in light scattering. The term itself refers to either loss of polarization or the generation of components orthogonal to the input fields. Hence, depolarization may originate from collisionally-induced rotations, collisional dipole-dipole interactions, electric torque acting on anisotropic electric polarization (in the case of anisotropic molecules), or electric torque acting on Kerr-induced anisotropy in isotropic molecules. Depolarization can also arise from magneto-electric interactions at the molecular level. Of these various processes, only dipole-dipole collisions, Kerr effects, and magneto-electric interactions can occur on timescales faster than the molecular re-orientation time. So these are the only candidates for explaining cross-polarized components in the *nonlinear* light scattering reported here. However, dipole-dipole interactions and Kerr effects yield radiation patterns that are very different from those measured experimentally in this work. Colliding molecules could instantaneously produce a depolarized probe field E_{probe}. In combination with a polarized pump field E_p this could perhaps mediate an optical Kerr effect [26] of the form $P=\varepsilon_0\chi^{(3)}E_{probe}E_pE_p$, but the angle-averaged polarization P would be zero in view of the random orientation of the probe field. At sufficiently high intensities, a Kerr effect based on a polarized probe (part of the input field) could in principle contribute importantly to co-polarized light scattering, though not to depolarized scattering. However, in this case, the three fields driving the nonlinearity would each contribute an angular projection to the radiation pattern. Hence the angular dependence of co-polarized light scattering would vary as $I(\theta)\sim\cos^6\theta$, resulting in a pattern which is not consistent with the data of Fig. 1. Dipole-dipole collisions and Kerr effects therefore do not

contribute significantly to our light scattering experiments. Hence, in isotropic media such as liquid CCl_4 only the magneto-electric mechanism can produce cross-polarized light on femtosecond timescales with both a simple dipolar and an unpolarized component as displayed in Fig. 1, in the non-relativistic intensity range of our experiments. Additionally, because of the small detection solid angle ($1.8x10^{-4}$ sr - see Appendix A), the geometrical effects such as projection of electric dipole components on the axis of cross-polarized detection, are negligible in these experiments.

Existing theory of magneto-electric interactions at the molecular level [14] suggests that they proceed as shown in Fig. 5. The process relies on establishing an electric polarization in the system with the optical *E* field and then converting the orbital angular momentum of the excited state to rotational angular momentum through a torque interaction driven by *H*. During the magnetic transition the angular momentum axis rotates as described in [14, 15], causing an enhancement of the induced magnetic moment. In Fig. 5(a), two magnetic transitions are indicated by downward red arrows. These two transitions are driven by frequency components of the incident pulse that are either at the carrier frequency or at a frequency shifted down by the molecular rotation frequency ω_ϕ. The former transition (dashed arrow) is detuned from resonance and is therefore expected to be polarization-preserving. The latter transition (solid arrow) resonantly stimulates a rotational excitation which causes depolarization of Stokes-shifted scattering on an ultrafast timescale. These two predictions are in excellent agreement with the results in Figs. 2 and 4 where the extra spectral features and their polarizations are evident. The radiation patterns of Fig. 1 are therefore in accord with the expectations of a magneto-electric interaction at the molecular level. Of equal significance, rotational features are present only in the MD scattered light spectra of Figs. 2 – 4 and they are unpolarized. This is in accord with the orientational averaging expected on the resonant magnetic transition (solid downward arrow in Fig. 5(a)) that generates them.

We note that the direct stimulation of depolarizing rotations by the resonant magnetic transition in Fig. 5(a) should cause "knock-on" vibrational excitations too. That is, the energy of a stimulated libration in combination with the energy of translation of a single molecule induces vibrations in neighboring molecules. This is consistent with the presence of Stokes-shifted *vibrational* features in the cross-polarized spectrum of Fig. 2. Moreover, the spectral features on the anti-Stokes or high- energy side of the spectrum in Fig. 2 are uniquely attributable to the "reverse" transition sequence depicted in Fig. 5(b) and can only result from a magneto-electric transition. Beginning from a thermal population in the first excited rotational state $|3\rangle$ at room temperature (labelled with rotational quantum number $J = 1$), a "reverse" magneto-electric transition annihilates a rotational quantum. This process yields an anti-Stokes rotational line but at the same time removes the rotational excitation necessary to cause "knock-on" vibrations during anti-Stokes scattering. Thus, anti-Stokes vibrational features are not expected and indeed no features are observed in the ED spectrum of Fig. 2 at vibrational shifts on the high frequency side of the carrier. On the other hand, a "reverse" transition originating from the second rotational energy level at room temperature can yield a second rotational anti-Stokes line (omitted from the schematic of Fig. 5(b) for simplicity). This transition accounts for the second anti-Stokes feature visible in the MD spectrum of Fig. 2, close to 1.6 eV.

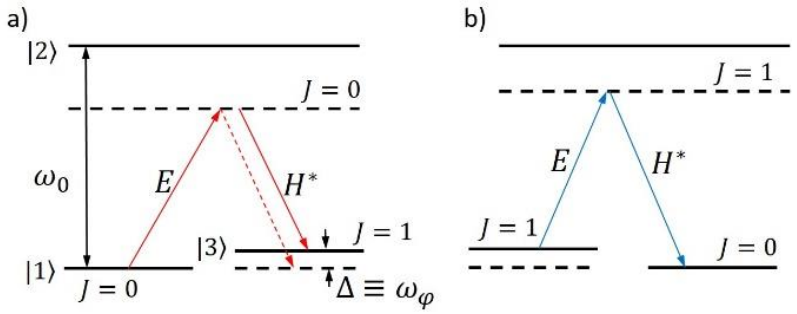

Fig. 5. Two-photon transitions responsible for second-order magneto-electric scattering driven by E and H fields. (a) In the Stokes process, the H field stimulates two classes of magnetic transition back to the ground state, as indicated by the two downward arrows. The magnetic transition at frequency $\omega - \omega_\phi$ (solid downward arrow) is resonant but can only be driven by a Fourier component of the optical pulse that is down-shifted from the carrier frequency by ω_φ. The first transition (dashed arrow) is ineffective in generating molecular rotations and produces polarized scattering. The second transition stimulates molecular rotations resonantly (final rotational state $J = 1$), causing unpolarized scattering and knock-on vibrations. (b) In the "reverse" process, the E field first drives an ED transition which preserves the initial rotational state ($J=1$) at room temperature. Then the magnetic field stimulates an anti-Stokes MD transition at frequency $\omega + \omega_\phi$ which removes the rotation. This generates unpolarized anti-Stokes rotational scattering without the possibility of knock-on vibrations. Note that anti-Stokes vibrational scattering is not observed in the MD spectrum of Fig. 2.

The magnetic torque interaction analyzed in [14, 15] enables magnetic transitions to take place at the optical frequency as indicated in Fig. 5. While the magnetic transitions, labelled by H^* in this figure, satisfy the quantum mechanical selection rules, they must also be ultrafast in order for the magneto-electric interaction to go to completion during the short pulse duration of our experiments. One can check that this requirement is met by turning to the quantum mechanical torque equation to estimate the time scale of magnetic torque dynamics. In the Heisenberg picture, the expectation value of torque expressed in terms of excited state orbital angular momentum L is

$$\left\langle \frac{dL_z}{dt} \right\rangle = \frac{i}{\hbar} Tr\{\tilde{\rho},\, [H^{(m)}, L_z]\}, \tag{1}$$

where $\tilde{\rho}$ is the slowly-varying amplitude of the density matrix. The magnetic torque Hamiltonian [14] is

$$H^{(m)} = (\hbar f L'_{-} O'_{+} a^{+} - h.c.), \tag{2}$$

Eq. (1) can be evaluated for the energy level picture of Fig. 5. As shown in appendix C, the torque equation then reduces to

$$\hbar/\tau = \mu_0^{(e)} E, \tag{3}$$

where τ is the characteristic time for completion of the dynamics and formation of the enhanced magnetic moment. Transition dipole moments of the tetrahalide series range from $\mu_0^{(e)} = 4.1 \times 10^{-30}$ $C.m$ for CCl_4 to $\mu_0^{(e)} = 11.3 \times 10^{-30}$ $C.m$ for $SiCl_4$ [27]. Consequently torque completion times for the various samples, at an intensity of $I = 10^{10}$ W/cm^2 (or $E = 1.94\times10^8$ V/m), comparable to our experimental intensities, are estimated to range from $\tau = 133$ fs down to $\tau = 48$ fs. The implication is that magnetic torque can indeed cause the exchange of orbital angular momentum for rotational angular momentum on an ultrafast timescale, allowing the magneto-electric interaction to go to completion during each pulse.

4. Conclusions

In summary, we have observed molecular rotations induced in a series of liquids composed of spherical top molecules on which optical electric fields are unable to exert torque, at intensities

far below any stimulated rotational Raman threshold. The rotational features that appear in cross-polarized (MD) spectra are unpolarized, showing that they do not originate from an ordinary Raman process. Instead they are uniquely attributable to the effect of the optical magnetic field, as predicted in recent quantum theory of molecular-scale magneto-electric interactions. We have excluded dipole-dipole collisions, Kerr effects, and geometrical effects as the potential explanations of the experimental observations. The observed intense radiant magnetization, therefore, is most likely explained by the inter-conversion of orbital and rotational angular momenta driven jointly by electric and magnetic optical fields. Magneto-electric torque dynamics increase the effective area enclosed by displacive polarization currents in dielectric media, readily yielding enhanced magnetic response as large as electric dipole response [13-15]. The polarization states of Stokes- and anti-Stokes librations and vibrations in inelastic light scattering spectra of tetrahedral molecules are entirely in accord with the current theory of magneto-electric interactions at the molecular level [13-15]. Thus we conclude that magneto-electric nonlinearities at the molecular level provide a new route for the control of molecular rotations, magnetic permeability and magnetic dispersion in dielectric media.

Appendix A: Experimental Setup

The light source for our scattering experiments was a regenerative amplified mode-locked Ti:sapphire laser. To investigate light scattering in tetrahedral molecules the collimated output beam was transmitted through a rotatable half-wave plate and polarizer combination to provide intensity control. The beam then passed through another polarization rotator ($\lambda/2$) that was computer-controlled and impinged on liquid samples prepared in sealed quartz cuvettes inside a light tight box. Light scattered at 90° was collected and collimated by a lens of focal length 15 cm. Several screens with irises were used to block stray light and limit the detection solid angle to 1.8×10^{-4} sr. An analyzer (polarizer) in the detection arm was used to select the polarization of transmitted signal light which was then softly focused on the cathode of an InGaAs photomultiplier (PMT) operated in photon-counting mode. Radiation patterns of scattered light were recorded by rotating the incident beam polarization through 360° in thirty-six steps while measuring the intensity of light transmitted by the analyzer under computer control. With the analyzer in the vertical position, electric dipole (ED) radiation patterns were measured in what we refer to as the co-polarized configuration, since the input laser polarization was vertical. Magnetic dipole (MD) radiation patterns were measured through a horizontally oriented analyzer in what we refer to as the cross-polarized configuration. The spectrum of scattered light could also be measured with a resolution of 0.01 nm by a 0.5 m Shamrock spectrometer fitted with a CCD camera (Andor Inc.) in the output plane.

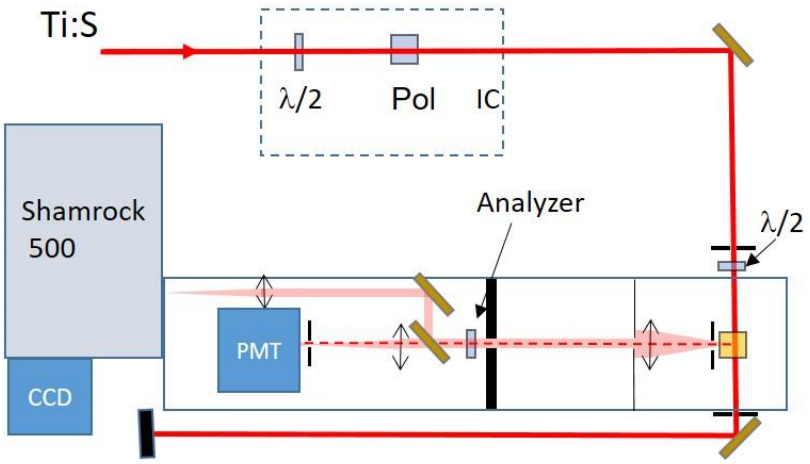

Fig. 6. Experimental setup. Ti:S = Ti:Sapphire laser, Pol = polarizer, IC = intensity controller. The analyzer is a rotating polarizer, which is set either vertical or horizontal polarization for detecting electric- or magnetic-dipole radiation patterns, respectively.

Appendix B: Sample preparation

The anhydrous chemicals used in this research were spectroscopic grade, purchased from Sigma Aldrich Inc., and were examined in quartz cuvettes with very high quality surfaces after rinsing with DI water, acetone, and isopropanol in a sequence and transferring them immediately to an oven, where they were heated at a temperature > 82 C for ~ 20 minutes. Cleaning and sealing of the cuvettes were performed inside a glovebox to prevent hydration of the samples. Just before each measurement, the four outer surfaces of the sample cuvette were given a final cleaning with optical tissue wetted with MeOH and blown dry using pressurized nitrogen gas.

Appendix C: Theoretical dynamics for torque completion time

The time required for the optical magnetic field to rotate the quantization axis of angular momentum in a molecule to rotational angular momentum, thereby enhancing its magnetic moment, was estimated with a classical argument in [14]. Here we provide a quantum derivation based on the torque Hamiltonian derived in that work.

In the Heisenberg picture, the expectation value for the rate of change of the *z*-projection of angular momentum due to an optical magnetic interaction for the basis of states 1, 2, and 3 shown in Fig. 5 is

$$\langle\tfrac{dL_z}{dt}\rangle = \tfrac{i}{\hbar} Tr\{\tilde{\rho}, [H^{(m)}, L_z]\}, \tag{4}$$

where $\tilde{\rho}$ is the slowly varying amplitude of the density matrix. The non-zero terms of the trace are

$$\langle\tfrac{dL_z}{dt}\rangle = \tfrac{i}{\hbar}\{\tilde{\rho}_{23}[H^{(m)}, L_z]_{32} + \tilde{\rho}_{32}[H^{(m)}, L_z]_{23}\}, \tag{5}$$

and the Hamiltonian for a magnetic dipole interaction including torque [14] is

$$H^{(m)} = \hbar f L'_- O'_+ a^+ + h.c. \tag{6}$$

In this expression f is the magnetic interaction strength, and $L'_{\mp}$, $O'_{\pm}$ and $a^{\pm}$ are raising and lowering operators for orbital and rotational angular momenta and the optical field respectively. The expectation of the rate of change of the *z*-projection of angular momentum may now be evaluated as

$$\langle\tfrac{dL_z}{dt}\rangle = \tfrac{i}{\hbar}\{-\tilde{\rho}_{23}\langle 3|L_z \hbar f L'_- O'_+ a^+|2\rangle + \tilde{\rho}_{32}\langle 2|\hbar f^* L'_+ O'_- a^- L_z|3\rangle\} = 2i\sqrt{n}\,\{f\tilde{\rho}_{23} + f\tilde{\rho}_{32}\}. \tag{7}$$

The magnetic interaction strength f depends on the electric field per photon ξ and the effective magnetic moment $\mu_{eff} = (\omega_0/\omega_c)\mu_0^{(m)}$, where ω_c is the cyclotron frequency and $\mu_0^{(m)} = (e\hbar/2m_e)$. The irreducible form of f is [14]

$$\hbar f = i\mu_{eff}\xi/c. \tag{8}$$

Once the effective magnetic moment acquires the enhanced value of $\mu_{eff} = c\mu_0^{(e)}/2$ as the result of the molecule exchanging orbital for rotational angular momentum, we find

$$f = i\mu_0^{(e)}\xi/2\hbar = ig/2. \tag{9}$$

Assuming the applied optical fields are high enough to generate the maximum value for the off-diagonal element of the density matrix, which is $\tilde{\rho}_{23} = \tilde{\rho}_{32} = \frac{1}{2}$ in a 2-level system, we finally obtain

$$\langle\tfrac{dL_z}{dt}\rangle = -|g|\sqrt{n}. \tag{10}$$

On the left side of the equation above, note that the *z*-projection of orbital angular momentum is only allowed to change by $\hbar$ during a magnetic dipole transition. If the characteristic time for completion of the torque dynamics responsible for enhanced magnetic response is designated by τ, the left side is given by $\langle\frac{dL_z}{dt}\rangle = -\frac{\hbar}{\tau}$ and the equation can be re-written as

$$\frac{\hbar}{\tau} = |g|\sqrt{n}. \tag{11}$$

Finally, since $\mu_0^{(e)}E = g\sqrt{n}$, one can solve for the torque completion time to obtain the result

$$\tau = \frac{\hbar}{\mu_0^{(e)}E}. \tag{12}$$

As stated in the main text, the timescale on which optical magnetic torque converts orbital angular momentum to rotational energy varies from $\tau = 133fs$ in CCl_4 to $\tau = 48fs$ in $SiCl_4$. The conclusion may therefore be drawn that magnetic torque can mediate the exchange of angular momentum on an ultrafast timescale, allowing a magneto-electric interaction in which both the electric and magnetic field components of the light cause transitions at the optical frequency during a single pulse, molecule by molecule.

Funding

MURI Center for Dynamic Magneto-optics, the Air Force Office of Scientific Research (FA9550-12-1-0119 and FA9550-14-1-0040); DURIP grant (FA9550-15-1-0307).

Acknowledgment

We thank H. Winful for useful discussions.

References

1. I. Levin, J. Li, J. Slutsker, A.L. Roytburd. “Design of Self-Assembled Multiferroic Nanostructures in Epitaxial Films”. Adv. Mater. **18**(15), 2044-2047 (2006).
2. J. Das, Y.Y. Song, N. Mo, P. Krivosik, C.E. Patton., “Electric-Field-Tunable Low Loss Multiferroic Ferrimagnetic–Ferroelectric Heterostructures”. Adv. Mater. **21**(20), 2045-2049 (2009).
3. N. Hur, S. Park, P.A. Sharma, J.S. Ahn, S. Guha, S.W. Cheong. “Electric polarization reversal and memory in a multiferroic material induced by magnetic fields”. Nature **429**, 392-395 (2004).
4. S.M. Wu, S.A. Cybart, P. Yu, M.D. Rossell, J. Zhang, R. Ramesh, R.C. Dynes. “Reversible electric control of exchange bias in a multiferroic field-effect device”. Nat. Mater. **9**, 756-761 (2010).
5. D. Bossini, K. Konishi, S. Toyoda, T. Arima, J. Yumoto, M.K.-Gonokami. “Femtosecond activation of magnetoelectricity”, Nat. Phys. **14**, 370-374 (2018).
6. V.V. Pavlov, R.V. Pisarev, A. Kirilyuk and Th. Rasing. “Observation of a transversal nonlinear magneto-optical effect in thin magnetic garnet films”. Phys. Rev. Lett. **78**(10), 2004 (1997).
7. M. Fiebig, D. Frohlich, T. Lottermoser, V.V. Pavlov, R.V. Pisarev, and H. –J. Weber. “Second harmonic generation in the centrosymmetric antiferromagnet NiO”. Phys. Rev. Lett. **87**(13), 137202 (2001).
8. C.D. Stanciu, F. Hansteen, A.V. Kimel, A. Kirilyuk, A. Tsukamoto, A. Itoh, T. Rasing. “All-optical magnetic recording with circularly polarized light”. Phys. Rev. Lett. **99**(4), 047601 (2007).
9. M. Fiebig. “Revival of the magnetoelectric effect”. J. Phys. D. Appl. Phys. **38**, R123-R152 (2005).
10. P. Curie. “Sur la symétrie dans les phénomènes physiques, symétrie d'un champ électrique et d'un champ magnétique”. J. Phys. (Paris) **3**(1), 393-415 (1894).
11. P. Debye. “Bemerkung zu einigen neuen Versuchen über einen magneto-elektrischen Richteffekt”. Z. Phys. **36**(4), 300-301 (1926).
12. K.Y. Bliokh, Y.S. Kivshar, and F. Nori. “Magnetoelectric effects in local light-matter interactions”. Phys. Rev. Lett. **113**(3), 033601 (2014).
13. A.A. Fisher, E.F.C. Dreyer, A. Chakrabarty, and S.C. Rand. “Optical magnetization, Part I: Experiments on radiant magnetization in solids”. Opt. Express **24**(23), 26055-26063 (2016).
14. A.A. Fisher, E.F.C. Dreyer, A. Chakrabarty, and S.C. Rand. “Optical Magnetization, Part II: Theory of induced optical magnetism”. Opt. Express **24**(23), 26064-26079 (2016).
15. E.F.C. Dreyer, A.A. Fisher, P. Anisimov, and S.C. Rand, “Optical magnetism, Part III: Theory of molecular magneto-electric rectification”, Optics Express **26**(14), 17755-17771 (2018).
16. J. Bucaro and T. Litovitz. “Rayleigh scattering: collisional motions in liquids”. J. Chem. Phys. **54**(9), 3846-3853 (1971).
17. J. McTague and G. Birnbaum. “Collision-induced light scattering in gaseous Ar and Kr”. Phys. Rev. Lett. **21**(10), 661 (1968).
18. L. Frommhold. “Collision-induced scattering of light and the diatom polarizabilities”. Adv. Chem. Phys. **46**, 1, (1981).

19. J. Stevens, G. Patterson, P. Carroll, and G. Alms. “The central Lorentzian in the depolarized Rayleigh spectra of CCl_4 and $GeCl_4$”. J. Chem. Phys. **76**(11), 5203-5207 (1982).
20. S. Shapiro and H. Broida. “Light scattering from fluctuations in orientations of CS_2 in liquids”. Phys. Rev. **154**(1), 129 (1967).
21. P. Madden. “The depolarized Rayleigh scattering from fluids of spherical molecules”. Mol. Phys. **36**(2), 365-388 (1978).
22. P.J. Chappell, M.P. Allen, R.I. Hallem, and D. Kivelson. “Theory of depolarized light scattering”. J. Chem. Phys. **74**(11), 5929-5941 (1981).
23. A.A. Fisher, E.F.C. Cloos, W.M. Fisher, and S.C. Rand, “Dynamic symmetry-breaking in a simple quantum model of magneto-electric rectification, optical magnetization, and harmonic generation”, Opt. Express **22**(3), 2910-2924 (2014).
24. W. Phadungsukanan, S. Shekar, R. Shirley, M. Sander, R.H. West, M. Kraft. “First principles thermochemistry for silicon species in the decomposition of tetraethoxysilane”. J. Phys. Chem. A **113**(31), 9041-9049 (2009).
25. T. Shinoda. “Qualitative classification of tetrahedral molecular crystals”. Mol. Cryst. Liquid *Cryst*. **76**, 191-197 (1981).
26. Y.R. Shen. *The Principles of Nonlinear Optics*. pp. 286-296 (J. Wiley & Sons)
27. G. Causley and B. Russell. “The vacuum ultraviolet absorption spectra of the group Iva tetrachlorides”. J. Electron Spectrosc. Relat. Phenom. **11**(4), 383-397 (1977).